

Damage Evaluation of Reinforced Concrete structures at lap splices of tensional steel bars using Bonded Piezoelectric Transducers

R. Regupathi^{a*} , C. Jayaguru^b 

^aDepartment of Civil Engineering, Government College of Engineering, Bodinayakanur, 625582, Tamil Nadu, India.
Email: regu.civil@gmail.com

^bDepartment of Civil Engineering, PSNA College of Engineering & Technology, Dindigul, 624622, Tamil Nadu, India.
Email: cjayaguru@psnacet.edu.in

* Corresponding author

<https://doi.org/10.1590/1679-78257069>

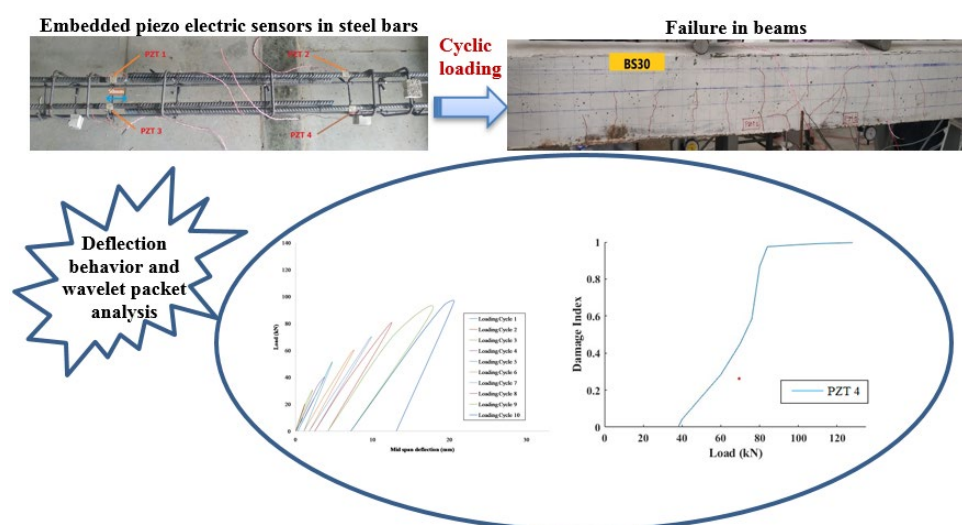
Abstract

Using bonded piezoelectric transducers (PZT), this study evaluates damage to reinforced concrete beams at lap splices of tensile rebars. Four reinforced concrete beams with a span of 2700mm and a cross-section of 200 x 250mm were cast and simply edge-supported on roller supports 2250mm apart. In the zone of constant moment, the tensile reinforcements of the beams were spliced with varying lap lengths (10 ϕ , 20 ϕ , 30 ϕ and 40 ϕ). Two PZT patches (one to operate as an actuator and the other as a receiver) were bonded on steel rebars and placed 50mm apart from their lapping edges. The wave propagation technique was used to record the signals experimentally, and the signals were processed further using wavelet packet analysis. By setting the time lag results of waves under pulse excitation, the damage of beams were identified. Damage indices were calculated based on the wavelet packet energy to ascertain the damage levels. The PZT was very sensitive to detect the pull-out bond failure and ductile flexural failure at the lap slices of steel rebars in the beam and it gives an advance indication before the structural collapse due to brittle failure.

Keywords

Lap Splices, PZT Transducers, Wave propagation, Damage Index, Pull-out bond, wavelet Packet

Graphical Abstract



Received: March 30, 2022. In Revised Form: April 01, 2022. Accepted: April 10, 2022. Available online: April 14, 2022

<https://doi.org/10.1590/1679-78257069>



Latin American Journal of Solids and Structures. ISSN 1679-7825. Copyright © 2022. This is an Open Access article distributed under the terms of the [Creative Commons Attribution License](https://creativecommons.org/licenses/by/4.0/), which permits unrestricted use, distribution, and reproduction in any medium, provided the original work is properly cited.

1 INTRODUCTION

The poor performance of reinforced concrete structures at various critical locations such as lapping zones of steel rebars and beam-column joints due to catastrophic consequences of failure has agreed on rigorous research interest for the past two decades. The failure of structures due to the insufficient lap length of the tension rebar is highly unpredictable and brittle. The adequate bond strength between the lap splice and the concrete core minimizes the likelihood of bar slippage or splitting failure prior to the yielding of reinforcing steel bars. Therefore, an effective structural health monitoring (SHM) technique is to be investigated at tension lap splices of steel rebar to detect the incipient failure of the RC structure. SHM using Piezoceramic or piezoelectric transducers (PZT) is an emerging and effective technique to detect the damages of RC structures which has the key characteristics like small size, lightweight, lower cost, active sensing, quick response and ease of implementation. It can be surface bonded or implanted in the structure with ease (Saafi, M., and Sayyah, T. (2001). The distinguishing property of Lead ZirconateTitanate PZT is that it generates surface charge in reaction to applied mechanical stress and deforms mechanically in response to an applied electric field. The PZT transducers are based either on electromechanical impedance (EMI) or electromechanical admittance (EMA) and wave propagation techniques are used for structural health monitoring (Shanker. R., et al., 2011), Venu Gopal., and Chee Kiong (2009), Mitra., et al. (2016). The above principles are based on the propagation of elastic waves in solids, where the stress waves are transferred into reinforcing steel rebar, steel girders, beams and plates. The mode shape of the propagated waves alters due to scattering and reflection when passed through a damaged region of the structure (Chen, X., and Chen, Y. (2020). Investigating the reflected and transmitted waves sensed by the PZT patches can provide comprehensive information on the damage (Zhang. J., et al., 2018).

Transducers made with piezoelectric lead zirconatetitanate (PZT) are increasingly being utilised to monitor the health of engineering structures like bridges and tall buildings. PZT transducers are embedded/surface bonded to monitor structures using electromechanical impedance (EMI) or electromechanical admittance (EMA) with a single PZT and wave propagation with multiple PZTs. Wave propagation technology with high voltage excitation can monitor a larger spectrum. The behaviour of reinforced concrete members at tension rebar lap splices is closely monitored since failure is unpredictable and brittle.

The early detection of deterioration to concrete structures using PZT patches than by LVDT and conventional microscopes demonstrates that SHM utilizing PZT patches is more robust than previous approaches. (Song. G., et al., (2007). Detecting incipient damage by the EMI technique is more sensitive and can be used for frequent interrogations of structures. Artificially induced debonding zones in concrete-filled steel tubes were effectively discovered using piezoceramics-based functional smart aggregates (SAs) implanted in concrete as actuators and PZT patches attached to the steel tube's surface as sensors. (Xu. D., et al., (2010). Voutetaki, M. E et al. (2016) tested five critical shear beams by varying spacing of web reinforcement to acquire EMA signals of PZT sensors for monitoring the shear failure of beams. It was demonstrated that transducers adjacent to diagonal cracking revealed sound differences between signals in the normal and damaged states. Several studies were carried out to detect the level of damages on plain concrete beams, slabs and mortar specimens using the root mean square deviation (RMSD) and the correlation coefficient deviation (CCD) (Xu, B., et al. (2013), Wang, D., et al., (2013), Hu, X., et al. (2014). A study of the electrical signals of elastic propagated waves recorded on healthy and artificially damaged steel bars revealed an accurate scaling of the analysed damage levels. (Karayannis, C. G., et al. (2016), Tawie, R., and Lee, H. (2010). PZT sensors were also applied to monitor the simulated corrosion damage of the rebars during the four-point bending test (Lu, Y., et al. (2013). Karayannis, C. G. et al., (2015) used EMA signals of PZT sensors to present flexural damages in steel bars at the bottom part of the mid-span section of a simply supported RC beam. Zhu, X. Q et al. (2013) conducted experiments on two RC slabs with varying debond lengths between reinforcing bars and concrete. To produce and perceive electric signals, piezoelectric components were bonded on reinforcing bars inserted in RC structures as actuators and sensors in this work. A plastic tube wrapped with rebar was used to replicate these debonds. The study also indicated that when debond duration increases, damage index (DI) values keeps increasing, whereas damage location has no influence.

Unfortunately, it is not feasible to have continuous reinforcing bars in concrete structures. It is because of handling and fabrication of steel, transportation limitation, steel weight, and space limitations in the reinforcing bar manufacturing factories. The splitting and brittle failure of concrete at lap splices of steel rebars are inevitable due to the inadequate lap length of reinforcing steel, insufficient confining reinforcement at lap zones and improper selection to position the lapping of reinforcing steel bars of RC structures (Farooq, Nakamura, & Miura, 2022). The post-earthquake studies reflect that the failure of the structural members also occurred at lap zones of steel reinforcing bars (Marques, D., et al. (2018). Therefore, more attention has to be given to the lap splice of reinforcing steel of the RC structures when subjected to cyclic loading (Karabinis, A. I. (2002).

This study focuses on the damage detection of the Reinforced Concrete beams at the lap splices of steel bars using PZT. To detect the damages on reinforced concrete structures at lap zones of steel bars, the PZT were mounted on steel bars with different lap lengths. Tests were performed in four reinforced concrete beams, where the tensile reinforcements of each beam were spliced with varying lengths of the lap of 10 times the diameter of a bar (10ϕ), 20 times diameter of a bar (20ϕ), 30 times diameter of a bar (30ϕ) and 40 times diameter of a bar (40ϕ) in the constant moment zone. Two PZT patches were mounted separately on each steel rebar (B1&B2) at lap splices; one PZT acted as an actuator to generate elastic waves which is then converted as electric signals and recorded by another PZT patch that acts as a sensor. The recorded signals were analyzed using wavelet packets as a signal processing tool.

1.1 SHM based on Wave Propagation Technique using PZTs

Recently, structural health monitoring employing wave propagation technique using PZT transducers has been given more attention and widely researched (Wilcox, P. D., et al., (2007), Giurgiutiu, V., and Soutis, C. (2010). The solution of governing equation of a guided wave mainly relies on the physical boundary conditions of the system (Azadi, M., et al. (2015). In most cases, the wave propagation technique propagates stress waves through steel rebars, beams, plates, and rails. The host structure's boundaries direct the stress waves and cause them to propagate along the length of the structure, where they may be sensed to detect the structure's damaged regions (Qin, Zhang, Xie, & Sun, 2019). The longitudinal guided wave has been used to differentiate the delamination of the RC interface as a function of signal length and mode (Yang, W., et al (2020). These waves will go further with less attenuation and provide a sensing range that is not observed by typical local NDE and global SHM approaches.

The proposed SHM approach was designed to detect possible damage in concrete structures at steel rebar lap splices. The PZT transducer was actuated for a particular frequency range by the arbitrary function generator (Tektronix AFG31000) the transmitted elastic waves and corresponding signals were captured by another PZT. These signals were recorded by a mixed-signal oscilloscope (Tektronix MSO 2000B, DPO 2000B) in the time domain. The recorded electric signals were analyzed using a wavelet packet to quantify the damage levels in the beams at the lap splice zone. The beam specimens were subjected to a cyclic loading paradigm. Before applying the load, the signal measurements were taken in the beam to utilize it as a reference.

Following that, measurements were taken at the peak load and then unloaded to 0 kN of each loading cycle. It is demonstrated that damage identification capacity significantly depends upon the effective frequency choice of the excitation rather than the voltage (Lim, Y.Y. et al. (2018), Zhang, J., et al. (2018).

A sweep sine signal with a frequency range of 10-100 kHz was used in this study. The signal had a magnitude of 20 V. At one end, the lap zone reinforcing was agitated, acting as a waveguide and surrounding concrete. The guided waves (Rose, J. L. (2014) were detected at the lap zone using bonded transducers on steel bars (B1 & B2). Since the steel bars were joined, these waves leaked into the concrete, causing the signal to attenuate before arriving the receiver at the lap zone's end of the other steel reinforcement (B2). Reflection, scatter, and mode conversion occur as a result of the de-bonding damage, further attenuating the waves.

2 PROPOSED METHOD OF STRUCTURAL HEALTH MONITORING (SHM)

2.1 Wavelet packet analysis

The recorded signals were investigated in this work utilizing wavelet packet analysis as a signal processing approach. The wavelet concept was initially applied to the examination of seismic data. Previously, Fourier Transform (FT) analysis was used to examine the signal data; however, wavelet packet analysis is currently used. The wavelet packet analysis splits the signal into shifting and scaling of wavelets formed at the origin, whereas the FT analysis splits it into sinusoidal waves of varying frequencies and stages.

Using a wavelet packet method, the PZT sensor detects sensor signals and decomposes them into sub-signals. The energy of the deconstructed signal is used to create the energy vector. The damage index is calculated by comparing the energy vector of the damaged state to the energy vector of the healthy state, which is used to measure the level of damage in concrete structures.

A step-by-step signal decomposition is done with approximation and precision in classical wavelet packet analysis. The signal approximation decomposes into another phase of approximation and precision at each step, and the process continues. In the N-level decomposition, there are N+1 methods to decompose or encode the signal. Each detail coefficient vector is also split into two parts as in approximation vector decomposition, which is a generalisation of wavelet decomposition in wavelet packet analysis. As a result, the wavelet packet analysis yields a more accurate

approximation and a complete binary tree. When using wavelet packet analysis to study the assessment of PZT sensors activated by wide frequency band, original signals can be decomposed in depth and insights on the high-frequency components can be retrieved using evidence from the high-frequency region measurement.

The 'sym8' wavelet packet was utilised in Matlab to breakdown the original PZT observations into three layers of wavelet packet in the current wavelet packet analysis (De la Rosa, et al). (2006). The adopted algorithm technique is consistent with that described by Xu, B., et al (2013). On one side of the specimen, the N_s number of PZT sensors is employed. The Voltage measurement signal V_k of PZT sensors is divided into $2N$ signal sets using N -level wavelet packet decomposition, as defined by the equation below.

$$V_k = v_{k,1} + v_{k,2} + \dots + v_{k,i} + \dots + v_{k,2^{N-1}} + v_{k,2^N} \quad (i=1, \dots, 2N), (k=1, \dots, N_s) \tag{1}$$

$v_{k,i}$ is time-series signal after wavelet packet decomposition and i indicates the frequency band index.

In this study, $N=3$. $v_{k,i}$ is further expressed as

$$v_{k,i} = [v_{k,i,1} v_{k,i,2} \dots v_{k,i,j} v_{k,i,M-1} v_{k,i,M}], (j=1, \dots, M) \tag{2}$$

Where M = Number of sampling data

Then, an energy vector corresponding to the PZT sensor k is defined and expressed as

$$\bar{E}_k = [e_{k,1} e_{k,2} \dots e_{k,i} \dots e_{k,2^{N-1}} e_{k,2^N}], (i=1, \dots, 2N) \tag{3}$$

Where $e_{k,i}$ is the corresponding energy of the decomposed signal, and it is defined as

$$e_{k,i} = \sum_{j=1}^M v_{k,i,j}^2, (i=1, \dots, 2N), (k=1, \dots, N_s) \tag{4}$$

Accordingly, the energy corresponding to each PZT sensor is defined as the 1-norm of the above energy vector as:

$$E_k = \sum_{i=1}^{2N} e_{k,i}, (k=1, \dots, N_s) \tag{5}$$

2.2 Damage Index (DI)

Considering civil structures, various damage indices were used for structural Health Monitoring systems. The root mean square deviation (RMSD) is the useful damage index for comparing the differences between the signals of a normal and damaged state. The RMSD between the PZT transducers' signals can be considered the most suitable damage index for detecting and characterization of damages in concrete structures [Bhalla, S.; Kaur, N., (2018)], Soh, C. K., et al., (2000), Tseng, K. K., and Naidu, A. S., (2002), Soh, C. K., et al., (2000). The damage index in this study is the RMSD between the energy vectors of the healthy and damaged states. At time i , the damage index equation is,

$$I = \sqrt{\frac{\sum_{j=1}^{2n} (E_{i,j} - E_{h,j})^2}{\sum_{j=1}^{2n} E_{h,j}^2}} \tag{6}$$

Where E_h is the Energy vector for a healthy state, $E_h = [E_{h,1}, E_{h,2}, \dots, E_{h,2n}]$.

The above equation represents the loss of transmission energy caused by the damages. The lower value of the damage index indicates an undamaged or healthy state and vice versa. Greater the damage index values, greater the damages.

3 EXPERIMENTAL WORK

Four concrete beams were tested with high-grade steel bars spliced in the constant moment region, with the objective of initiating failure in the tension zone. The RC beams were cast as a singly reinforced rectangular section with a cross-section of 200mm x 250mm and a length of 2700mm. It was simply supported and subjected to a four-point bending test. As illustrated in Figure 1, two high-grade steel deformed bars of 16mm diameter were used as tension

reinforcement and two numbers of 12mm diameter were used as compression reinforcement on all four specimens. The tension reinforcement was spliced with different lap lengths of 10ϕ , 20ϕ , 30ϕ and 40ϕ which were designated as BS10, BS20, BS30 and BS40 respectively.

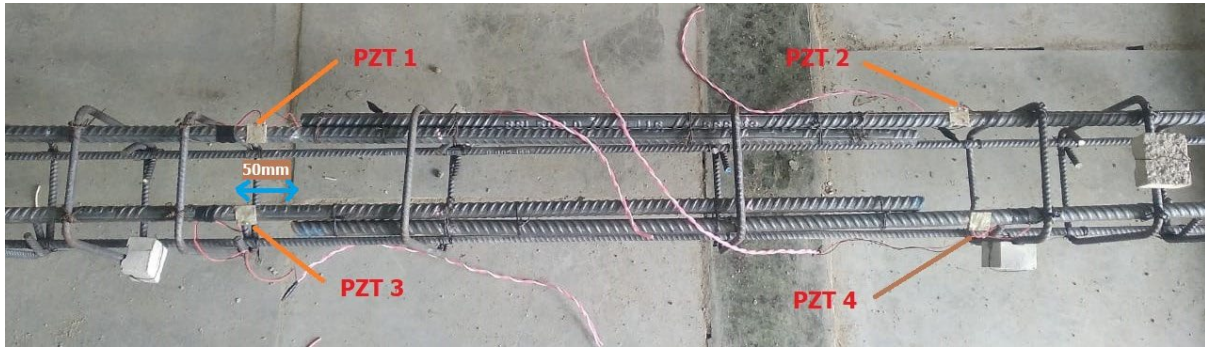


Figure 1 Mounted PZT patches in the spliced rebars

The concrete mix was proportioned with 370kg/m³ of ordinary Portland cement, 185 kg/m³ of water, 814 kg/m³ of sand and 1140 kg/m³ of coarse aggregate with a maximum aggregate size of 20mm and 0.5 of water-cement ratio. The measured compressive strength of concrete was 32 N/mm². Four PZT patches of 20mm X 20mm X 0.4mm dimension (PZT 1, PZT 2, PZT3 and PZT 4) were attached on the spliced bars at 50mm apart from its lapping edges, as shown in Figure 2. On steel rebar, PZT 1 & PZT 3 were utilized as actuators to produce high frequency waves, and PZT 2 & PZT 4 were used as sensors to receive and record the electric signals.They were bonded properly on the steel bar using epoxy adhesive. A fine coating of epoxy coating was provided as a waterproof covering to the installed PZT transducers to prevent damage during concrete casting. The longitudinal section of the beam reinforcement detailing is shown in Figure and the location of installed PZT transducers Figure 3.

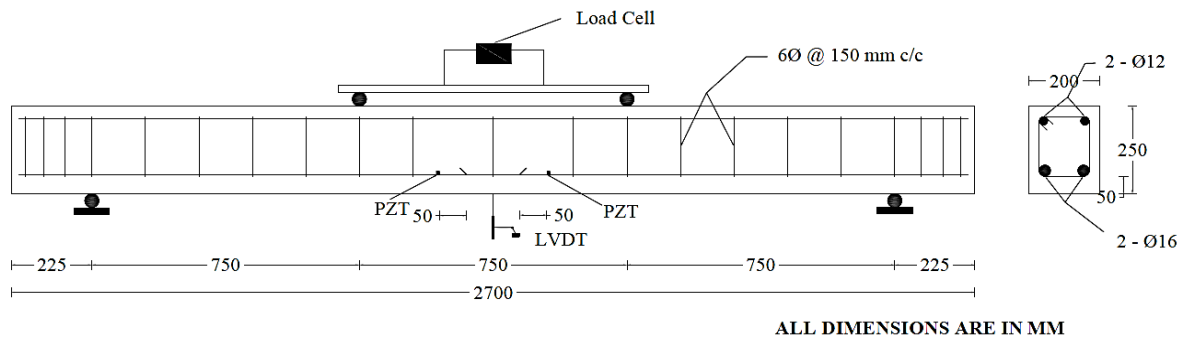


Figure 2 Reinforcement detailing of RC beam

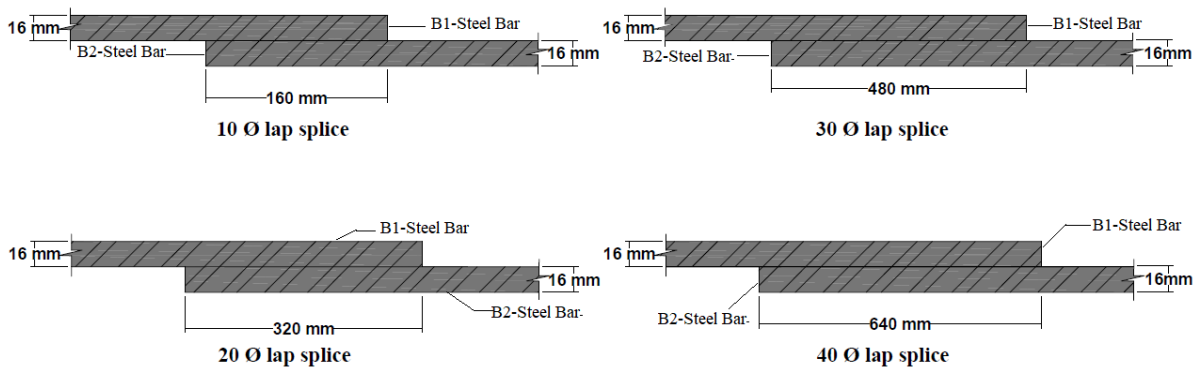


Figure 3 Details of Lap splice

In this investigation, a cyclic loading paradigm was used. Initially, the structure was loaded to 10 kN and unloaded to 0 kN. After that, the load value was gradually increased and unloaded to 0 kN and continued up to the failure load of 42 kN

for the beam of 10ϕ lap splice, 68 kN for the beam of 20ϕ lap splice, 96 kN for the beam of 30ϕ lap splice and 128 kN for the beam of 40ϕ lap splice. The hydraulic jack exerts load at the centre, distributed evenly at two loading points of the beam, as shown in Figure 4. After each loading, the initiation of crack and its propagation was observed and traced on the surface of the beam to identify the type of failure. The deflections in the centre of the span were measured with a precision of 0.01mm using a Linear Variable Differential Transducer (LVDT). Throughout the tests, load and deflection measurements were continuously monitored and documented. In the time domain, the signals were generated by function generators and recorded by mixed-signal oscilloscopes. Electric signals of 20V magnitude in the form of sweep sine waves were used to actuate the PZT 1 and PZT 3 at the same time. The PZT 2 and PZT 4 transmitted and received elastic waves generated by the PZT 1 and PZT 3. Furthermore, using the experimental set-up established in the SHM technique, measurements of the electric signals in terms of volts were recorded on the installed PZT 2 and PZT 4 of four beams at every cycle loading using the experimental set-up illustrated in Figure 5.



Figure 4 Experimental test set-up of the beams incorporated with PZTs

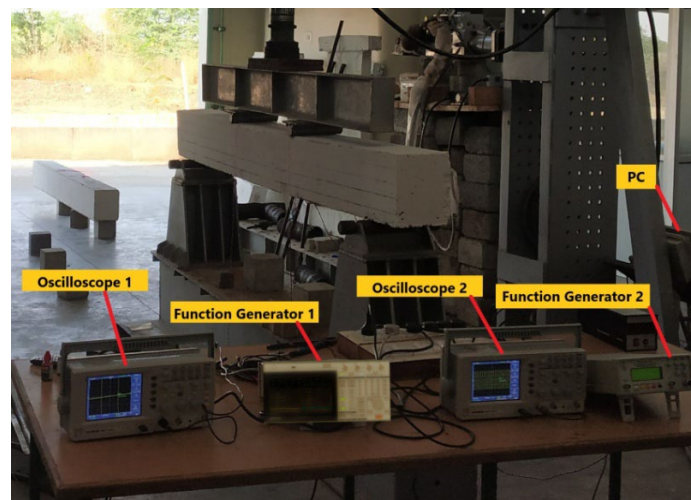


Figure 5 Instrumentation of SHM set-up

4 Results and Discussion

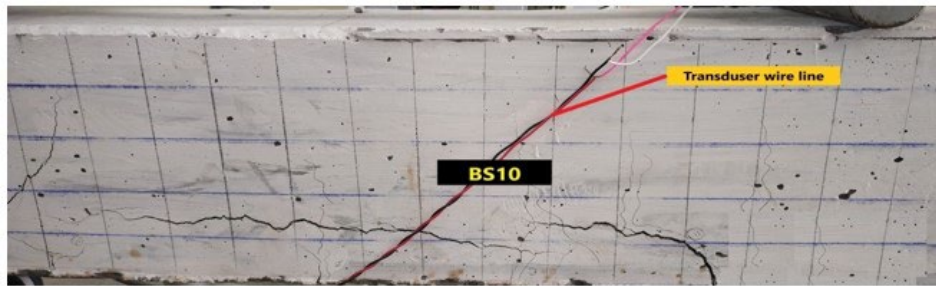
4.1 Mode of Failure

The initiation of flexural cracks in all the beams were observed within the region with constant moment, predominantly occurring in the section of spliced ends as shown in Figure 6. The type of failure, cracking load, ultimate load and corresponding central deflection of the tested beams are provided in Table 1. On increasing the load of the beam, additional cracks were raised within and outside the constant moment region. In BS10 and BS20 beams, the beam specimens of splice length 10ϕ and 20ϕ showed longitudinal splitting cracks initiated at the bottom that extended to the beam's side, as shown in Figures 6(a) and 6(b). A medium splice (BS30) and a long splice (BS40) beams led to flexural failure. In the constant moment area, the cracks started at the bottom and progressed vertically as flexural cracks. Other

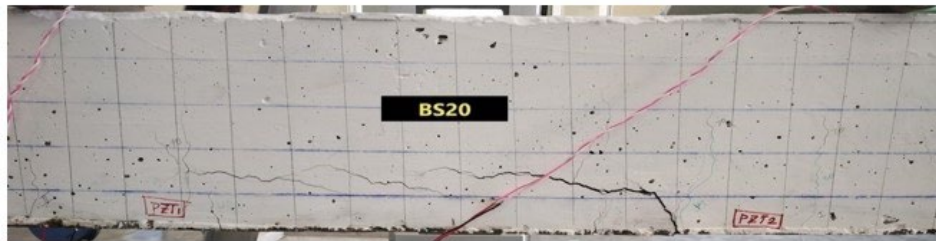
than the constant moment area, flexural-shear cracks were noticed.6(c) and 6(d) shows the crack patterns of BS30 and BS40 beams, respectively.

Table 1 Type of Failure in BS10, BS20, BS30 and BS40

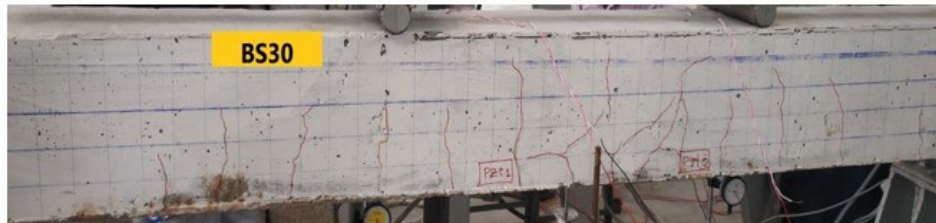
Beam	First cracking stage		Final stage		Type of failure
	Cracking load (kN)	Deflection (mm)	Ultimate load (kN)	Deflection (mm)	
BS10	22	3.4	42	4.7	Splitting
BS20	28	7.8	68	13.3	Splitting
BS30	42	9.3	96	22.6	Flexure
BS40	48	8.7	128	31.1	Flexure



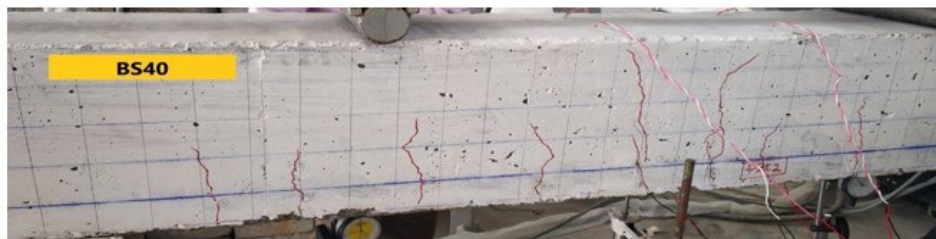
a) Splitting cracks in BS10 Beam



b) Splitting cracks in BS20 Beam



c) Flexural-shear Cracks in BS30



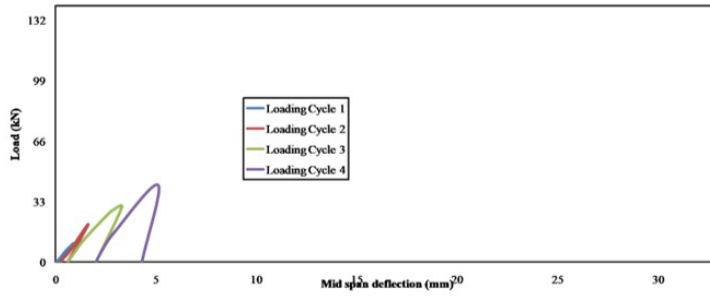
d) Flexural-Shear cracks in BS40

Figure 6 Crack patterns of BS10, BS20, BS30 and BS40

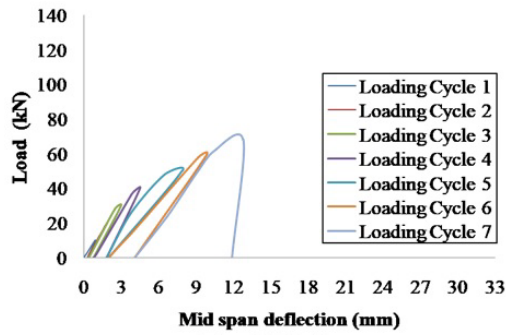
4.2 Load vs. Deflection

Figure 7 presents that with increasing number of cycles and increase in lap length, the bond resistance between steel and concrete at lap splices increases. It was observed that the first two cycles of loading in beams BS10 and BS20 and the first four cycles of loading in beams BS30 and BS40 exhibited flexural-ductile nature. Alike, Figure (a) and Figure (b) show the drastic load drop after reaching the ultimate load in the last loading cycle. This evidence concludes that the beams BS10 and BS20 failed in brittle nature due slippage at bond at lap splices. After the fourth cycle of loading in beams

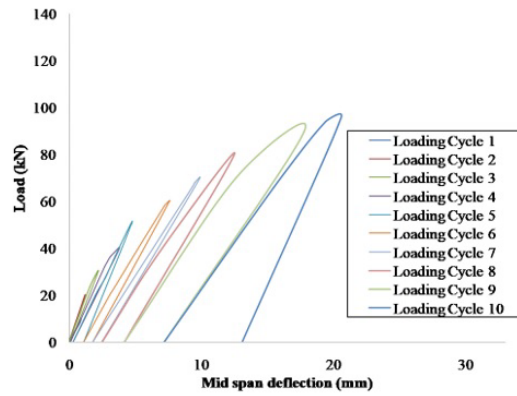
BS30 and BS40, there was an increase in residual deflection at mid-span. Figures 7(c) and 7(d) illustrate the beam's gradual yielding after attaining the ultimate point.



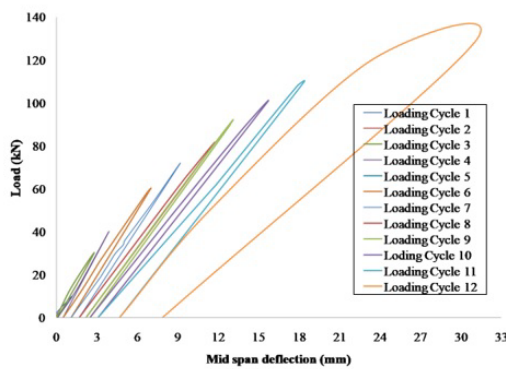
a) BS10 Beam



b) BS20 Beam



c) BS30 Beam



d) BS40 Beam

Figure 7 Loading vs mid-span deflection of BS10, BS20, BS30 and BS40 Beams

4.3 Structural Health Monitoring

Sweep sinusoidal signals were used to stimulate piezoceramic actuators (PZT1 and PZT3) during the loading process, while piezoceramic patches (PZT2 and PZT 4) were used as health monitoring and damage detection sensors. At a sampling frequency of 100 kHz, a sweep sine signal with a frequency range of 10kHz to 100kHz was applied with a signal magnitude of 20 Volts.

4.3.1 TimeDomain Analysis of Signals

The Beams BS10 and BS20 experienced four cycles of loading and seven loading cycles, respectively. The PZT2 and PZT4 were used to record the signals from the excitation of PZT1 and PZT3. Before applying the load on beams, the signals were recorded from the sensors, and they were used as reference signals (healthy state condition). The sensor readings were taken at two points in each loading cycle, one at the peak and the other at the release of load at 0kN. The time-domain plots of recorded signals from PZT2 of beams BS10 and BS40 are shown in Figures 8 and 9.

The output magnitude of the PZT2 sensor decreased with increase in load values. At the initial stages of the loading cycle, the maximum sensor output magnitude of 5.2V was observed in beam BS40, while in the final loading cycle, it was close to 0V. It represented that the reinforced concrete beam gave a good conduit for the propagation of waves in the first loading cycle, but in the final loading cycle, the wave propagation is almost blocked. Therefore, the RC beam was in a healthy state at the first loading cycle and a damaged condition in the final loading cycle.

It is observed that the amplitudes of sensor measurements vary between the peak of loading and release of loading to 0kN in loading cycles 4 to 7. When the load reached the peak of these cycles, the cracks were opened, and the path of elastic waves was obstructed and scattered. Thus the amplitudes of signals decreased. Subsequently, when the load was released to 0kN, the opened cracks closed and the amplitude of waves increased. It shows that the beam specimen behaved as a quasi-elastic state in the respective loading cycles. After each loading cycle, the new cracks were developed, the old cracks were widened, and hence the amplitude of signals has reduced further.

The variations in amplitudes of sensor measurements between the peak of loading and release of loading to 0kN as in beam BS40 were not found anywhere in the beam specimen BS10 can be seen in 8. It illustrates that the beam BS10 is not having quasi-elastic behavior since it failed in brittle nature.

The abrupt drop in the sensor responses signifies that the sharp increase in the crack width is due to failure in the specimen. Because of the final loading cycle of BS40, there is a plunge in the sensor output mainly due to flexural-shear cracks in the concrete beam. These cracks were observed due to a severe blockage in the propagation of waves.

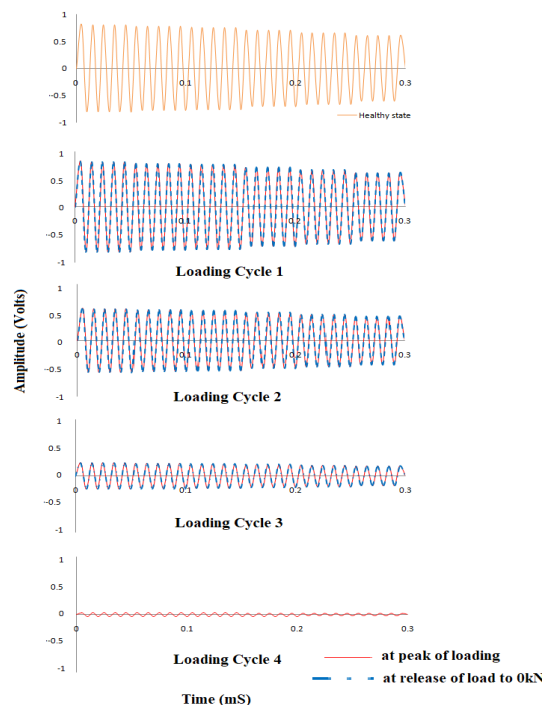


Figure 8 Time domain Response of PZT2 for Beam BS10

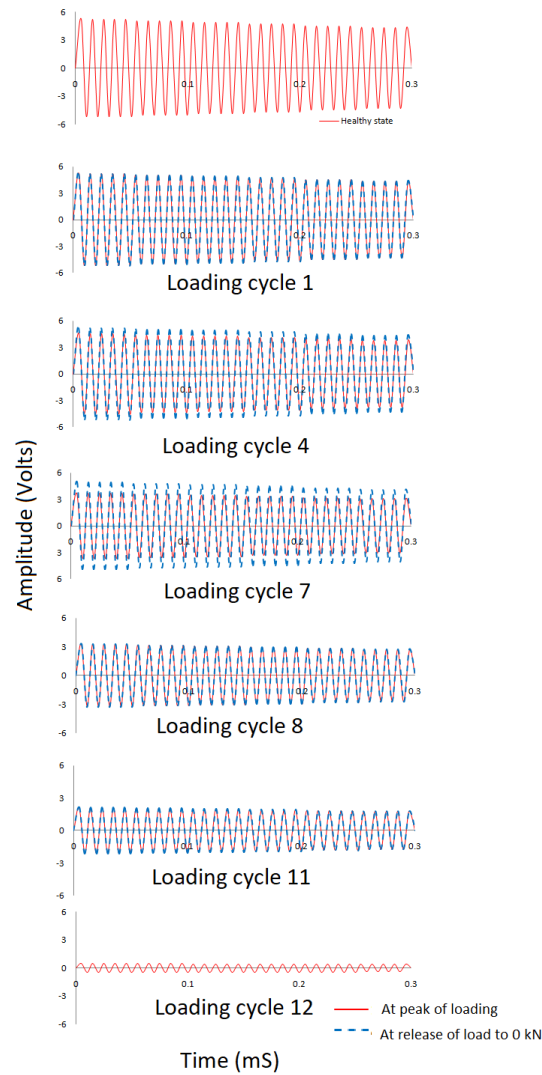


Figure 9 Time domain Response of PZT2 for Beam BS40

4.3.2 Damage Index

The acquired signals of each beam from the sensors PZT2 and PZT4 when PZT1 and PZT3 as actuators were decomposed using wavelet packet analysis and the corresponding energy vectors were derived. The damage indices for all tested beams were calculated as discussed in section 2 and listed in Table 2 to Table 5.

Table 2 Damage index value of PZT sensors for beam BS10 (Beam of 10φ lap splice) with PZT1 and PZT3 as actuator

Load Designation	Peak Load value of each cycle in kN	Damage Index	
		PZT2	PZT4
Loading Cycle 1	10	0	0
Loading Cycle 2	12	0	0.0231
Loading Cycle 3	14	0.02653	0.04346
Loading Cycle 4	18	0.19425	0.21234
Loading Cycle 5	20	0.22764	0.242766
Loading Cycle 6	22	0.25347	0.263428
Loading Cycle 7	24	0.97962	0.989362
Loading Cycle 8	30	0.98129	0.989362
Loading Cycle 9	40	0.99234	0.995745
Loading Cycle 10	42	0.99574	0.995745

Table 3 Damage index value of PZT sensors for Beam BS20 (Beam of 20φ lap splice) with PZT1 and PZT3 as actuator

Load Designation	Peak Load value of each cycle in kN	Damage Index	
		PZT2	PZT4
Loading Cycle 1	10	0	0
Loading Cycle 2	14	0	0
Loading Cycle 3	16	0.02345	0
Loading Cycle 4	20	0.07342	0.06015
Loading Cycle 5	24	0.15894	0.136749
Loading Cycle 6	30	0.25671	0.225564
Loading Cycle 7	34	0.32063	0.297345
Loading Cycle 8	36	0.97456	0.984962
Loading Cycle 9	40	0.98564	0.984962
Loading Cycle 10	50	0.98872	0.992481
Loading Cycle 11	60	0.99123	0.995489
Loading Cycle 12	68	0.99774	0.99762

Table 4 Damage index value of PZT sensors for Beam BS30 (Beam of 30φ lap splice) with PZT1 and PZT3 as actuator

Load Designation	Peak Load value of each cycle in kN	Damage Index	
		PZT2	PZT4
Loading Cycle 1	10	0	0
Loading Cycle 2	20	0	0
Loading Cycle 3	26	0	0
Loading Cycle 4	30	0.05643	0
Loading Cycle 5	40	0.15786	0.130435
Loading Cycle 6	44	0.220867	0.202789
Loading Cycle 7	50	0.29453	0.277174
Loading Cycle 8	56	0.36099	0.387544
Loading Cycle 9	60	0.45362	0.467391
Loading Cycle 10	66	0.64037	0.650935
Loading Cycle 11	68	0.85765	0.83459
Loading Cycle 12	70	0.90121	0.90459
Loading Cycle 13	72	0.95734	0.98913
Loading Cycle 14	80	0.96742	0.98913
Loading Cycle 15	90	0.98566	0.99456
Loading Cycle 16	96	0.99728	0.99712

Table 5 Damage index value of PZT sensors for Beam BS40 (Beam of 40φ lap splice) with PZT1 and PZT3 as actuator

Load Designation	Peak Load value of each cycle in kN	Damage Index	
		PZT2	PZT4
Loading Cycle 1	10	0	0
Loading Cycle 2	20	0	0
Loading Cycle 3	30	0	0
Loading Cycle 4	34	0	0
Loading Cycle 5	38	0	0.0432
Loading Cycle 6	40	0.04213	0.07419
Loading Cycle 7	50	0.16346	0.19677
Loading Cycle 8	60	0.28363	0.30161
Loading Cycle 9	70	0.45168	0.46451
Loading Cycle 10	76	0.58547	0.60645

Table 5 Continued...

Load Designation	Peak Load value of each cycle in kN	Damage Index	
		PZT2	PZT4
Loading Cycle 11	80	0.86782	0.84290
Loading Cycle 12	82	0.92011	0.91249
Loading Cycle 13	84	0.97474	0.98709
Loading Cycle 14	90	0.97895	0.98709
Loading Cycle 15	100	0.98579	0.99032
Loading Cycle 16	110	0.99126	0.99354
Loading Cycle 17	120	0.99437	0.99677
Loading Cycle 18	128	0.99677	0.99677

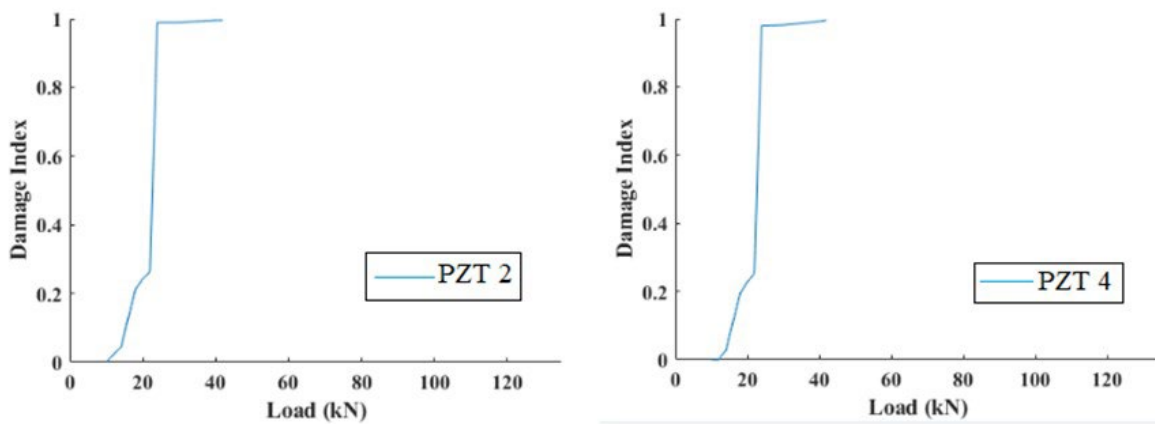


Figure 10 Damage Index Versus Load for the sensors PZT 2 and PZT 4 of Beam BS10

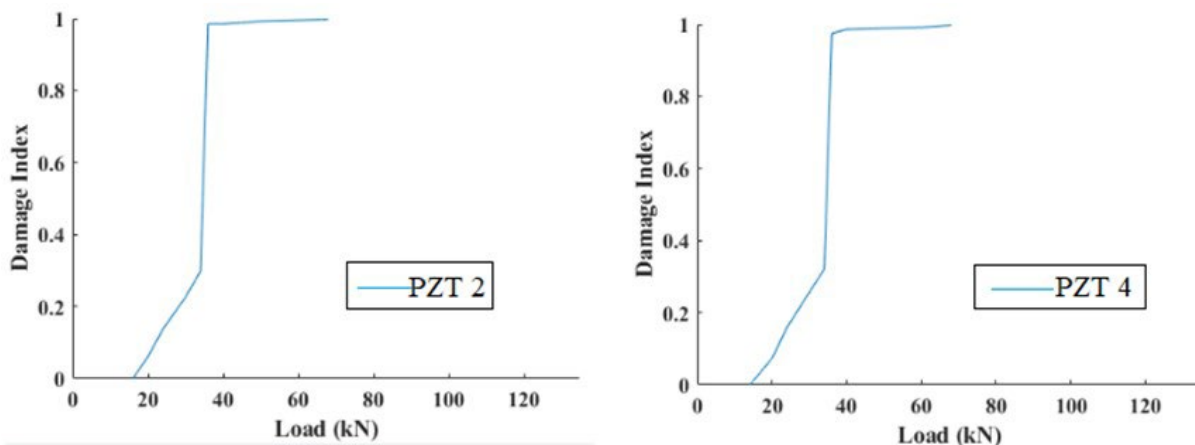


Figure 11 Damage Index Versus Load for the sensors PZT 2 and PZT 4 of Beam BS20

It is apparent from Figures 10 and 11 that the DI values for sensors PZT2 and PZT4 of the beams BS10 and BS20 starts to increase when the load value reaches to 10kN and 16kN, respectively, which indicates that the internal circumferential tensile cracks around the lapped steel bars are initiated and increased further in the concrete. The longitudinal splitting cracks are detected by a microscope when the load values reach 22kN and 28kN, respectively. Therefore, the proposed method is more sensitive since it can sense the internal cracks even before the splitting cracks appear on the beam surfaces.

When the load values reach 24kN and 36kN in the beams BS10 and BS20 (Beams of 10φ and 20φ lap splices) respectively, the DI value for each sensor surpasses its maximum value, followed by a sudden vertical climb of damage index curve from 0.3 to 1 as shown in the Figures 10 and 11. It indicates that the complete splitting and pull-out bond failure occurred in the beams of 10φ and 20φ lap splices, respectively.

The value of damage index 1 shows sensor output as zero, it indicates the cracks blocks all the wave propagation. However, based on the experiment results, it is observed that the structures failed at 42kN and 68kN, respectively. Therefore, the proposed method of SHM is more beneficial to detect the pull-out bond failure of structures where the lap length of steel bars is poorly detailed. Also, it may give an advance indication even before the structural collapse due to brittle failure.

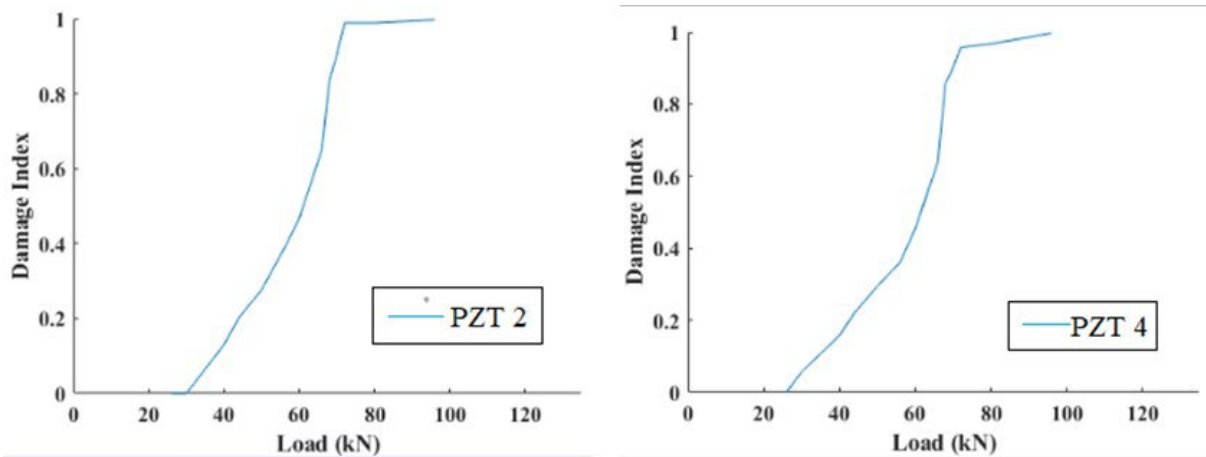


Figure 12 Damage Index Versus Load for the sensors PZT 2 and PZT 4 of Beam BS30

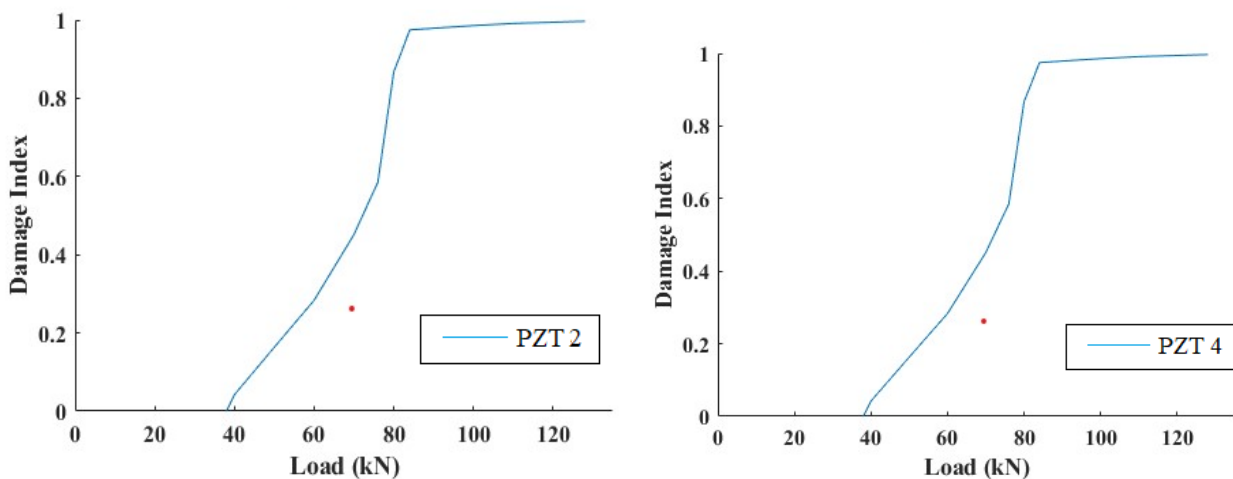


Figure 13 Damage Index Versus Load for the sensors PZT 2 and PZT 4 of Beam BS40

From Figures 12 and 13, the DI values for sensors PZT2 and PZT4 start to escalate when the load value extends to 30kN and 36kN in the beams BS30 and BS40, respectively. It also shows that the DI value rises progressively with the increase of the load, and the maximum DI value of 1 was attained at 72kN and 84kN of the beams, respectively. These indicates that there was an adequate bond resistance developed between concrete and steel bars at lap splices and there was no catastrophic failure of beams BS10 and BS20. However, the complete failure of beams was detected using conventional devices at lap splices only when the load value reached 96kN and 128kN, respectively. Hence the proposed SHM is more sensitive to detecting the damages at lap zones of steel bars in RC structures.

5 CONCLUSIONS

This paper is a validating empirical investigation, that is, a research into whether the active sensing approach based on the PZT transducer can successfully identify failure at lap splices of of tensile rebars in RC concrete beams. Based on the detailed SHM evaluation on the use of bonded PZT at lap splices of tensile rebars in concrete beams, the following conclusions are made.

1. The piezoelectric-based transducers can be applied to measure the condition of RC structures at steel bar lap splices. During cyclic loading, whenever a crack occurs in the beam, the transmission energy between the actuator and the sensor drops drastically. The transmission energy-based damage index suggested in the study is a better indicator for detecting the presence and severity of internal cracks.
2. The PZT was very sensitive to detect the pull-out bond failure and ductile flexural failure at the lap slices of steel rebars in the beam.
3. The amplitudes of sensor measurements varied between the peak of loading and unloading. When the load reached the peak of these cycles, the cracks were opened, and the path of elastic waves was obstructed and scattered. Thus the amplitudes of signals decreased. The abrupt drop in the sensor responses signifies that the sharp increase in the crack width is due to failure in the specimen.
4. The suggested method detects the presence and growth of cracks more efficiently. It also supports the detection of complete damage of the structure earlier than conventional methods. In addition, it may give an advance indication even before the structural collapse due to brittle failure.

Author's Contributions: Conceptualization, R Regupathi and C Jayaguru; Methodology, R Regupathi and C Jayaguru; Investigation, R Regupathi; Writing - original draft, R Regupathi; Writing - review & editing, R Regupathi; Funding acquisition, R Regupathi; Resources, R Regupathi; Supervision, C Jayaguru.

Editor: Marcílio Alves

References

- Azadi, M., Azadi, E., and Fazelzadeh, S. A. (2015). Control of a support excitation smart beam subjected to a follower force with piezoelectric sensors/actuators. *Latin American Journal of Solids and Structures*, 12(12), 2403-2416. doi:10.1590/1679-78252047
- Bhalla, S., and Kaur, N. (2018). Prognosis of low-strain fatigue induced damage in reinforced concrete structures using embedded piezo-transducers. *International Journal of Fatigue*, 113, 98-112. doi:10.1016/j.ijfatigue.2018.04.002
- Chen, X., and Chen, Y. (2020). Experimental study on damage identification of nano-sio2 concrete filled GFRP tube column using piezoceramic transducers. *Sensors*, 20(10), 2883. doi:10.3390/s20102883
- De la Rosa, J. J., Lloret, I., Moreno, A., Puntonet, C., and Górriz, J. (2006). Wavelets and wavelet packets applied to detect and characterize transient alarm signals from termites. *Measurement*, 39(6), 553-564. doi:10.1016/j.measurement.2005.11.021
- Farooq, U., Nakamura, H., & Miura, T. (2022). Evaluation of failure mechanism in lap splices and role of stirrup confinement using 3D RBSM. *Engineering Structures*, 252, 113570. doi:10.1016/j.engstruct.2021.113570
- Giurgiutiu, V., and Soutis, C. (2010). Guided Wave Methods for Structural Health Monitoring. *Encyclopedia of Aerospace Engineering*. doi:10.1002/9780470686652.eae187
- Hu, X., Zhu, H., and Wang, D. (2014). A study of concrete slab damage detection based on the electromechanical impedance method. *Sensors*, 14(10), 19897-19909. doi:10.3390/s141019897
- Karabinis, A. I. (2002). Reinforced concrete beam-column joints with lap splices under cyclic loading. *Structural Engineering and Mechanics*, 14(6), 649-660. doi:10.12989/sem.2002.14.6.649
- Karayannis, C. G., Chalioris, C. E., Angeli, G. M., Papadopoulos, N. A., Favvata, M. J., and Providakis, C. P. (2016). Experimental damage evaluation of reinforced concrete steel bars using piezoelectric sensors. *Construction and Building Materials*, 105, 227-244. doi:10.1016/j.conbuildmat.2015.12.019
- Karayannis, C. G., Voutetaki, M. E., Chalioris, C. E., Providakis, C. P., and Angeli, G. M. (2015). Detection of flexural damage stages for RC beams using piezoelectric sensors (PZT). *Smart Structures and Systems*, 15(4), 997-1018. doi:10.12989/sss.2015.15.4.997
- Lim, Y. Y., Smith, S. T., and Soh, C. K. (2018). Wave propagation based monitoring of concrete curing using piezoelectric materials: Review and Path Forward. *NDT and E International*, 99, 50-63. doi:10.1016/j.ndteint.2018.06.002
- Lu, Y., Li, J., Ye, L., and Wang, D. (2013). Guided waves for damage detection in rebar-reinforced concrete beams. *Construction and Building Materials*, 47, 370-378. doi:10.1016/j.conbuildmat.2013.05.016

- Marques, D., Flor, F. R., Medeiros, R. D., Pagani Junior, C. D., and Tita, V. (2018). Structural Health Monitoring of Sandwich structures based on dynamic analysis. *Latin American Journal of Solids and Structures*, 15(11). doi:10.1590/1679-78254309
- Mitra, M., and Gopalakrishnan, S. (2016). Guided Wave based Structural Health Monitoring: A Review. *Smart Materials and Structures*, 25(5), 053001. doi:10.1088/0964-1726/25/5/053001
- Qin, F., Zhang, Z., Xie, B., & Sun, R. (2019). Experimental study on damage detection in ECC-concrete composite beams using piezoelectric transducers. *Sensors*, 19(12), 2799. doi:10.3390/s19122799
- Rose, J. L. (2014). Guided waves in anisotropic media. *Ultrasonic Guided Waves in Solid Media*, 276-293. doi:10.1017/cbo9781107273610.017
- Saafi, M., and Sayyah, T. (2001). Health monitoring of concrete structures strengthened with advanced composite materials using piezoelectric transducers. *Composites Part B: Engineering*, 32(4), 333-342. doi:10.1016/s1359-8368(01)00017-8
- Shanker, R., Bhalla, S., Gupta, A., and Praveen Kumar, M. (2011). Dual use of PZT patches as sensors in global dynamic and local electromechanical impedance techniques for structural health monitoring. *Journal of Intelligent Material Systems and Structures*, 22(16), 1841-1856. doi:10.1177/1045389x11414219
- Soh, C. K., Tseng, K. K., Bhalla, S., and Gupta, A. (2000). Performance of smart piezoceramic patches in health monitoring of a RC Bridge. *Smart Materials and Structures*, 9(4), 533-542. doi:10.1088/0964-1726/9/4/317
- Song, G., Gu, H., Mo, Y. L., Hsu, T. T., and Dhonde, H. (2007). Concrete structural health monitoring using embedded piezoceramic transducers. *Smart Materials and Structures*, 16(4), 959-968. doi:10.1088/0964-1726/16/4/003
- Tawie, R., and Lee, H. (2010). Piezoelectric-based non-destructive monitoring of hydration of reinforced concrete as an indicator of bond development at the steel-concrete interface. *Cement and Concrete Research*, 40(12), 1697-1703. doi:10.1016/j.cemconres.2010.08.011
- Tseng, K. K., and Naidu, A. S. (2002). Non-parametric damage detection and characterization using smart piezoceramic material. *Smart Materials and Structures*, 11(3), 317-329. doi:10.1088/0964-1726/11/3/301
- Venu Gopal Madhav Annamdas, & Chee Kiong Soh. (2009). Application of electromechanical impedance technique for engineering structures: Review and future issues. *Journal of Intelligent Material Systems and Structures*, 21(1), 41-59. doi:10.1177/1045389x09352816
- Voutetaki, M. E., Papadopoulos, N. A., Angeli, G. M., and Providakis, C. P. (2016). Investigation of a new experimental method for damage assessment of RC beams failing in shear using piezoelectric transducers. *Engineering Structures*, 114, 226-240. doi:10.1016/j.engstruct.2016.02.014
- Wang, D., Song, H., and Zhu, H. (2013). Numerical and experimental studies on damage detection of a concrete beam based on PZT admittances and correlation coefficient. *Construction and Building Materials*, 49, 564-574. doi:10.1016/j.conbuildmat.2013.08.074
- Wilcox, P. D., Konstantinidis, G., Croxford, A. J., and Drinkwater, B. W. (2007). Strategies for guided wave structural health monitoring. *AIP Conference Proceedings*. doi:10.1063/1.2718139
- Xu, B., Zhang, T., Song, G., and Gu, H. (2013). Active interface debonding detection of a concrete-filled steel tube with piezoelectric technologies using wavelet packet analysis. *Mechanical Systems and Signal Processing*, 36(1), 7-17. doi:10.1016/j.ymsp.2011.07.029
- Xu, D., Cheng, X., Huang, S., and Jiang, M. (2010). Identifying technology for structural damage based on the impedance analysis of piezoelectric sensor. *Construction and Building Materials*, 24(12), 2522-2527. doi:10.1016/j.conbuildmat.2010.06.004
- Yang, W., Yang, X., and Li, S. (2020). Monitoring of interfacial debonding of concrete filled pultrusion-GFRP tubular column based on piezoelectric smart aggregate and wavelet analysis. *Sensors*, 20(7), 2149. doi:10.3390/s20072149
- Zhang, J., Li, Y., Huang, Y., Jiang, J., Ho, S. (2018). A feasibility study on timber moisture monitoring using piezoceramic transducer-enabled active sensing. *Sensors*, 18(9), 3100. doi:10.3390/s18093100
- Zhu, X. Q., Hao, H., Fan, K. Q. (2013). Detection of delamination between steel bars and concrete using embedded piezoelectric actuators/sensors. *Journal of Civil Structural Health Monitoring*, 3(2), 105-115. doi:10.1007/s13349-013-0039-2.